Geophys. J. Int. (2016) **205,** 1165–1179
GJI Geodynamics and tectonics
doi: 10.1093/gji/ggw077

Residual polar motion caused by coseismic and interseismic deformations from 1900 to present

G. Cambiotti,[1] X. Wang,[2] R. Sabadini[1] and D.A. Yuen[3,4]

[1] *Department of Earth Sciences, University of Milan, Milan, Italy. E-mail: gabriele.cambiotti@unimi.it*
[2] *Institute of Geology and Geophysics, Chinese Academy of Sciences, Beijing, China*
[3] *Department of Earth Sciences, University of Minnesota, Minneapolis, MN, USA*
[4] *Minnesota Supercomputing Institute, Minneapolis, MN, USA*

Accepted 2016 February 21. Received 2016 February 20; in original form 2015 November 24

SUMMARY

We challenge the perspective that seismicity could contribute to polar motion by arguing quantitatively that, in first approximation and on the average, interseismic deformations can compensate for it. This point is important because what we must simulate and observe in Earth Orientation Parameter time-series over intermediate timescales of decades or centuries is the residual polar motion resulting from the two opposing processes of coseismic and interseismic deformations. In this framework, we first simulate the polar motion caused by only coseismic deformations during the longest period available of instrumental seismicity, from 1900 to present, using both the CMT and ISC-GEM catalogues. The instrumental seismicity covering a little longer than one century does not represent yet the average seismicity that we should expect on the long term. Indeed, although the simulation shows a tendency to move the Earth rotation pole towards 133°E at the average rate of 16.5 mm yr^{-1}, this trend is still sensitive to individual megathrust earthquakes, particularly to the 1960 Chile and 1964 Alaska earthquakes. In order to further investigate this issue, we develop a global seismicity model (GSM) that is independent from any earthquake catalogue and that describes the average seismicity along plate boundaries on the long term by combining information about present-day plate kinematics with the Anderson theory of faulting, the seismic moment conservation principle and a few other assumptions. Within this framework, we obtain a secular polar motion of 8 mm yr^{-1} towards 112.5°E that is comparable with that estimated from 1900 to present using the earthquake catalogues, although smaller by a factor of 2 in amplitude and different by 20° in direction. Afterwards, in order to reconcile the idea of a secular polar motion caused by earthquakes with our simplest understanding of the seismic cycle, we adapt the GSM in order to account for interseismic deformations and we use it to quantify, for the first time ever, their contribution to polar motion. Taken together, coseismic and interseismic deformations make the rotation pole wander around the north pole with maximum polar excursions of about 1 m. In particular, the rotation pole moves towards about Newfoundland when the interseismic contribution dominates over the coseismic ones (i.e. during phases of low seismicity or, equivalently, when most of the fault system associated with plate boundaries is locked). When megathrust earthquakes occur, instead, the rotation pole is suddenly shifted in an almost opposite direction, towards about 133°E.

Key words: Seismic cycle; Earth rotation variations; Plate motions; Seismicity and tectonics; Dynamics: seismotectonics.

1 INTRODUCTION

The potential effect of earthquakes on the displacement of the Earth rotation axis has been studied by the pioneering works of Mansinha & Smylie (1967), Smylie & Mansinha (1968), Dahlen (1973) and Chao & Gross (1987), in terms of both Chandler wobble excitation and secular polar motion, defined as the motion of the rotation pole, the latter coinciding with the point where the rotation axis pierces the Earth's surface. Chao & Gross (1987) and Zhou *et al.* (2013) simulated the cumulative effect of earthquakes on the

secular polar motion by implementing the CMT catalogue (Dziewonski & Anderson 1981; Ekström *et al.* 2012) from 1977 to 1985 into self-gravitating spherically symmetric non-rotating elastic isotropic (self-gravitating SNREI) Earth models. Chao *et al.* (1996) and Soldati *et al.* (2001) repeated this simulation considering the cumulative effect of earthquakes until 1993 and 1997, respectively. All these studies found that the secular polar motion due to earthquakes is smaller by about one or two orders of magnitude than the observation of 10 cm yr^{-1} towards 75°W (McCarthy & Luzum 1996) and points in the almost opposite direction.

The occurrence of megathrust earthquakes in the last decade (the 2004 Sumatra, 2010 Maule and 2011 Tohoku earthquakes) leads naturally to reconsider the importance of seismicity on the secular polar motion (Gross & Chao 2006; Xu *et al.* 2014), possibly until now underestimated since we have been looking at a too short time interval. This was already noticed by Chao & Gross (1987) considering the calculations of rotation pole shift due to the 30 largest earthquakes from 1900 to 1964 (including the 1960 Chile and 1964 Alaska earthquakes) by O'Connell & Dziewonski (1976). They indeed obtained a secular polar motion of 13 cm yr^{-1} towards 148°E that is comparable in amplitude, although almost opposite in direction, with the observation of 10 cm yr^{-1} towards 75°W.

The first goal of the present work is to revisit the simulation of polar motion caused by earthquakes implementing the longest period available of instrumental seismicity into self-gravitating SNREI Earth models, since the beginning of the past century to present, combining the CMT (Dziewonski & Anderson 1981; Ekström *et al.* 2012) and ISC-GEM (Storchak *et al.* 2013) catalogues. In this way we mitigate, as much as possible, the impact of the shortness, in time, of the implemented earthquake catalogue on our conclusions. This issue is particularly important nowadays in view of recent findings by Nakada *et al.* (2015), who compared the contributions to the secular polar motion, or true polar wander, from past and present-day ice mass changes. In fact, we must verify whether or not earthquakes can induce polar motion comparable with that due to these surface ice loadings. From the analysis of Earth Orientation Parameters (EOP) time-series from modern space measurement techniques (Lunar and Satellite Laser Ranging and Very Long Baseline Interferometry), it will be also possible to discriminate between the different sources of polar motion excitation by determining breaks in the prograde circular motion of the rotation pole corresponding to sudden excitations associated with large seismic events (Smylie & Zuberi 2009; Smylie *et al.* 2015).

Our second and main goal consists in reconciling the idea of a secular polar motion caused by earthquakes with our understanding of the seismic cycle. Indeed, considering only the cumulative effect of coseismic deformations on polar motion leaves out all those contributions from closely related physical processes, particularly the strain accumulation during interseismic periods. This is important because, in first approximation and on average, coseismic and interseismic deformations cancel out each other, leaving only steady block motions of adjacent plates (Savage & Burford 1973; Savage 1983; Segall 2010). As it concerns the rotational dynamics of the Earth, we thus expect that, on the long term, the cumulative perturbation of the Earth inertia due to the earthquake sequence is compensated by that due to interseismic deformations and, so, coseismic and interseismic deformations, taken together, cannot contribute to secular polar motion. From this perspective, it is evident that what we shall simulate and, hopefully, observe in EOP time-series on timescales of decades or centuries is not a secular polar motion caused by earthquakes. Rather, it is the residual polar motion resulting from the two opposite processes of coseismic and interseismic deformations.

All previous studies about the secular polar motion caused by earthquakes did not consider the complementary process of interseismic deformations, now included in our analysis. In order to tackle this new issue, we develop a global seismicity model (GSM) which describes the long-term slip rate over the fault system associated to the plate boundaries on the basis of information on present-day plate kinematics and on the argument that the relative motion between plates is accommodated by both seismic and aseismic slip (Davies & Brune 1971; Anderson 1975; Kagan 2002). Then, according to the back slip strategy for modelling interseismic deformations, proposed first by Savage & Burford (1973) and Savage (1983) and successively applied to regional studies by Prawirodirdjo *et al.* (1997), Murray & Segall (2001), McCaffrey (2002) and Meade & Hager (2005), we will use this GSM for quantifying the perturbation of the Earth inertia due to interseismic deformations at the global scale. Particularly, following Savage & Burford (1973) and Savage (1983) (see also Segall 2010), the modelling of interseismic deformations will be achieved by imposing a constant (in time) slip rate on the fault system associated to the plate boundaries that is opposite to the average slip rate necessary to accommodate plate motion. In this way, for the first time, we will simulate the secular polar motion due to interseismic deformations and, in the end, combining it with that obtained by implementing CMT and ISC-GEM catalogues, we will obtain the residual polar motion due to both coseismic and interseismic deformations since the beginning of the past century.

Since this is the first attempt to investigate polar motion caused by the seismic cycles at the global scale, we will simply consider a basic sketch of the seismic cycle, that is, the model of elastic rebound. For the sake of simplicity, we thus omit the effect of viscoelastic relaxation of stress by viscous flow, already discussed in previous studies, although outside the framework of the seismic cycle (Yuen & Peltier 1982; Soldati & Spada 1999).

2 POLAR MOTION CAUSED BY GLOBAL SEISMICITY OF THE PAST FOUR DECADES

The Global CMT Project (http://www.globalcmt.org) provides the point-like seismic sources (i.e. the hypocentre and the seismic moment tensor) by inversion of teleseismic waves for all earthquakes with moment magnitude $M_w \gtrsim 6$ in 1976, $M_w \gtrsim 5.7 \sim 5.4$ from 1977 to 2003 and $M_w \gtrsim 5$ from 2004 to present (Dziewonski *et al.* 1981; Ekström *et al.* 2012). For the case of the 2004 Sumatra earthquake is also available a multiple CMT solution composed by five point-like seismic sources (Tsai *et al.* 2005) that we will use for replacing the relevant solution in the CMT catalogue. In order to model the polar motion due to this earthquake sequence, we resort to the linearized equations governing the rotational dynamics of the deformable Earth (Munk & MacDonald 1960; Lambeck 1980) and we compute the perturbation of the Earth inertia due to each earthquake by means of self-gravitating SNREI Earth models and within the framework of the elastic dislocation theory (Dahlen 1973; Smylie *et al.* 1979; Chao & Gross 1987; Cambiotti & Sabadini 2015). We use the stratification of the elastic parameters and density of the Preliminary Reference Earth model (PREM, Dziewonski & Anderson 1981) and take into account for ocean water redistribution by means of an infinitesimally thin uniform global ocean layer (Cambiotti *et al.* 2011a; Cambiotti & Sabadini 2013).

2.1 Mathematical formulation

According to this theoretical framework, we assume that the Earth is in hydrostatic equilibrium and rotating around the axis crossing the north pole before the earthquake sequence. We then identify the mean position of the rotation pole (averaged over a few Chandler wobble periods) by means of a unit vector $\hat{\boldsymbol{m}}$ that we decompose into its initial position and the infinitesimal perturbation

$$\hat{\boldsymbol{m}} = \hat{\boldsymbol{x}}_3 + \delta\hat{\boldsymbol{m}}. \tag{1}$$

Here $\hat{\boldsymbol{x}}_3$ is the unit vector pointing towards the north pole and $\delta\hat{\boldsymbol{m}}$ is the infinitesimal perturbation describing the polar motion and is customary expressed in terms of the direction cosines m_1 and m_2

$$\delta\hat{\boldsymbol{m}} = m_1\,\hat{\boldsymbol{x}}_1 + m_2\,\hat{\boldsymbol{x}}_2 \tag{2}$$

with $\hat{\boldsymbol{x}}_1$ and $\hat{\boldsymbol{x}}_2$ being the Cartesian unit vectors parallel to the equatorial plane and pointing towards the 0° and 90°E meridians, respectively.

From the linearized equations governing the rotational dynamics of the elastic Earth (Munk & MacDonald 1960; Lambeck 1980), the direction cosines are obtained as follows:

$$m_i = \frac{1}{1 - k_2^{\mathrm{T,E}}/k_2^{\mathrm{T,F}}}\,\frac{\Delta \mathrm{I}_{i3}}{C - A} \qquad \forall\, i = 1, 2, \tag{3}$$

where $C - A \approx 1.88\, M_{\mathrm{E}}\, a^2$ is the difference between the maximum and minimum inertia moments of the rotating Earth in hydrostatic equilibrium (with M_{E} and a being the Earth mass and radius; Chambat *et al.* 2010), $k_2^{\mathrm{T,E}}$ and $k_2^{\mathrm{T,F}}$ are the elastic and fluid tidal gravitational Love numbers of spherical harmonic degree 2 (Cambiotti *et al.* 2011b) and $\Delta \mathrm{I}_{i3}$ are the following components of the perturbation of the deviatoric inertia tensor of the Earth, $\Delta\mathbf{I}$, caused by the earthquake

$$\Delta \mathrm{I}_{i3} = \hat{\boldsymbol{x}}_i \cdot \Delta\mathbf{I} \cdot \hat{\boldsymbol{x}}_3 \qquad \forall\, i = 1, 2. \tag{4}$$

Particularly, the ratio $k_2^{\mathrm{T,E}}/k_2^{\mathrm{T,F}}$ describes the amount of the hydrostatic rotational bulge which readjusts to new positions of the rotation axis by elastic deformations.

Following Chao & Gross (1987) and Cambiotti & Sabadini (2015), we can express the perturbation of the Earth moment of inertia caused by a point-like seismic source like the sum of contributions associated with the polar, bipolar and quadrupolar patterns (i.e. of spherical harmonic orders 0, ±1 and ±2, respectively) of the seismic perturbation of spherical harmonic degree 2. Particularly, as discussed in appendix A, it can be written as follows:

$$\Delta \mathrm{I}_{i3} = M_{\mathrm{E}}\, a^2 \sum_{p=0}^{2} k_{2,p}^{\mathrm{D}}(r)\, B_i^p \qquad \forall\, i = 1, 2, \tag{5}$$

where $k_{2,0}^{\mathrm{D}}$, $k_{2,1}^{\mathrm{D}}$ and $k_{2,2}^{\mathrm{D}}$ are the gravitational seismic Love numbers governing the local incremental gravitational potential at the Earth surface associated with the polar, bipolar and quadrupolar patterns of the seismic perturbation, respectively, and r is the radial distance from the Earth centre (radius from now on) of the hypocentre. Furthermore, B_i^p ($i = 1, 2$; $p = 0, 1, 2$) are non-dimensional factors which depend on the seismic moment tensor (divided by the shear modulus evaluated at the hypocentre depth) and on the angular coordinates of the epicentre (in the geographic reference frame). Their expressions are given in Appendix A, eq. (A5).

Fig. 1 shows the seismic Love numbers as function of the hypocentre depth $z = a - r$, from the Earth surface down to 700 km, that is about the maximum depth in the CMT catalogue. We note that $k_{2,0}^{\mathrm{D}}$ and $k_{2,2}^{\mathrm{D}}$ are characterized by step-like discontinuities in correspondence of the discontinuities of the elastic parameter of PREM

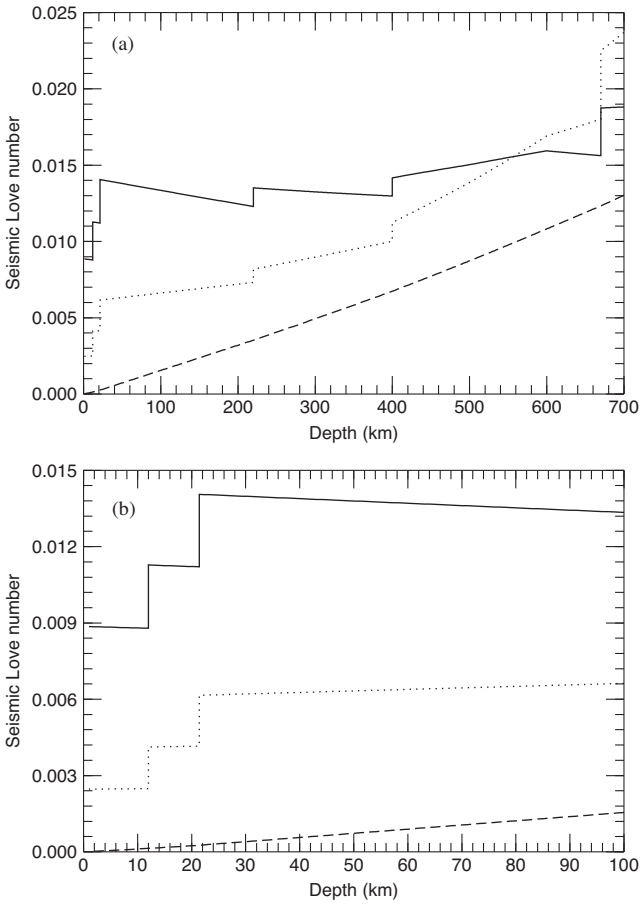

Figure 1. Seismic Love numbers $-k_{2,0}^{\mathrm{D}}$, $k_{2,1}^{\mathrm{D}}$ and $k_{2,2}^{\mathrm{D}}$ (solid, dashed and dotted lines, respectively) as function of the hypocentre depth $z = a - r$ from the Earth surface down to (a) 700 km and (b) 100 km. Note that, for the sake of the graphical representation, we plot the negative of seismic Love number associated with the polar pattern of seismic perturbation, $-k_{2,0}^{\mathrm{D}}$.

(i.e. at the lower-upper crust and Moho discontinuities and at the 220 km, 400 km and 670 km discontinuities). This is consistent with the specific expressions of the discontinuity of the spheroidal vector solution for these two Love numbers that, indeed, depends on the elastic parameters at the hypocentre depth (see eq. (28b,d) of Cambiotti & Sabadini 2015). Differently, $k_{2,1}^{\mathrm{D}}$ is continuous across the internal interfaces of the Earth model because its expression for the discontinuity of the spheroidal vector solution does not depend on the elastic parameters at the hypocentre depth (see eq. (28c) of Cambiotti & Sabadini 2015). Furthermore, this Love number is about proportional to depth and varies from zero at the Earth surface to values comparable with the other two Love numbers by increasing depth. In this respect, the perturbation of the Earth inertia associated with the bipolar pattern becomes important only for deep earthquakes.

These results agree with those of Dahlen (1973, see his fig. 1) who obtained similar expressions for the perturbation of the Earth inertia in terms of three Green functions, denoted with Γ_1, Γ_2 and Γ_3 in that study. The latter coincide with our seismic Love numbers (except for constant factors) and it can be shown that $\Gamma_1 \propto k_{2,2}^{\mathrm{D}}$, $\Gamma_2 \propto k_{2,0}^{\mathrm{D}}$ and $\Gamma_3 \propto k_{2,1}^{\mathrm{D}}$. However, we note that, differently from Dahlen (1973), our seismic Love numbers are defined for every harmonic degree (Cambiotti & Sabadini 2015) and not only for the

spherical harmonic degree 2 involved in the rotational dynamics of the Earth.

2.2 Results

Fig. 2 shows the polar motion obtained by implementing the CMT catalogue. The total polar shift accumulated since 1976 amounts to 37.1 cm and points towards 121.0°E. It corresponds to almost one centimetre per year (9.4 mm yr^{-1}), with the largest contributions coming from the three megathrust earthquakes occurred in the last decade: the 2004 Sumatra, 2010 Maule and 2011 Tohoku earthquakes (see Table 1).

In considering the temporal evolution of the accumulated polar shift, we note that its direction is quite stable and points towards about 120°E. On the other hand, the rate of growth of the polar shift amplitude is characterized by a marked increase with time (Fig. 2b). In fact, by dividing the four decades spanned by the CMT catalogue into three periods (from 1976 to 1993, from 1994 to 2003 and from 2004 to present), we obtain average rates of polar shift which grow from a period to another by about a factor of 5, as reported in Table 2. This large variability of polar motion is due to the fact that the seismicity of the past four decades varied considerably from one decade to another, particularly as it concerns the magnitude of the earthquakes occurred in each decade. In this respect, for each period, Table 2 reports also the seismic moment rate, $\partial_t M_s$, that is the total seismic moment, M_s, accumulated in a time interval, T, divided by the time interval itself

$$\partial_t M_s = \frac{M_s}{T}. \tag{6}$$

Henceforth, ∂_t stands for the derivative with respect to time and should be intended as the incremental ratio on time intervals much larger than the duration of a seismic event.

This simulation of polar motion updated to the last release of the CMT catalogue confirms the results of previous works based only on the first two decades of the CMT catalogue (Chao & Gross 1987; Chao *et al.* 1996; Spada 1997; Soldati *et al.* 2001): the global seismicity has the general tendency to display the rotation pole towards about 120°E. Particularly, this tendency is not much affected by variations of the intensity of seismicity from one decade to another, namely whether giant earthquakes occur or not. Rather, as pointed out by Spada (1997) and restated at the end of this section within the present formalism, it depends on the geographical location of plate boundaries and, particularly, of subduction zones from which comes the main contribution to global seismicity. On the other hand, these variations of the intensity of seismicity have a large impact on the rate of polar motion that, indeed, varies significantly with time (Fig. 2b and Table 2), while the direction varies of about 14° from the first and last periods.

We consider separately the contributions to polar motion from each pattern of the seismic perturbations and discriminating between interplate (depth less than 50 km and within 220 km from plate boundaries), intraplate (depth less than 50 km and far from plate boundaries more than 220 km) and deep (depth greater than 50 km) earthquakes, as shown in Supporting Information Figs S1 and S2, we note that the contribution from interplate earthquakes

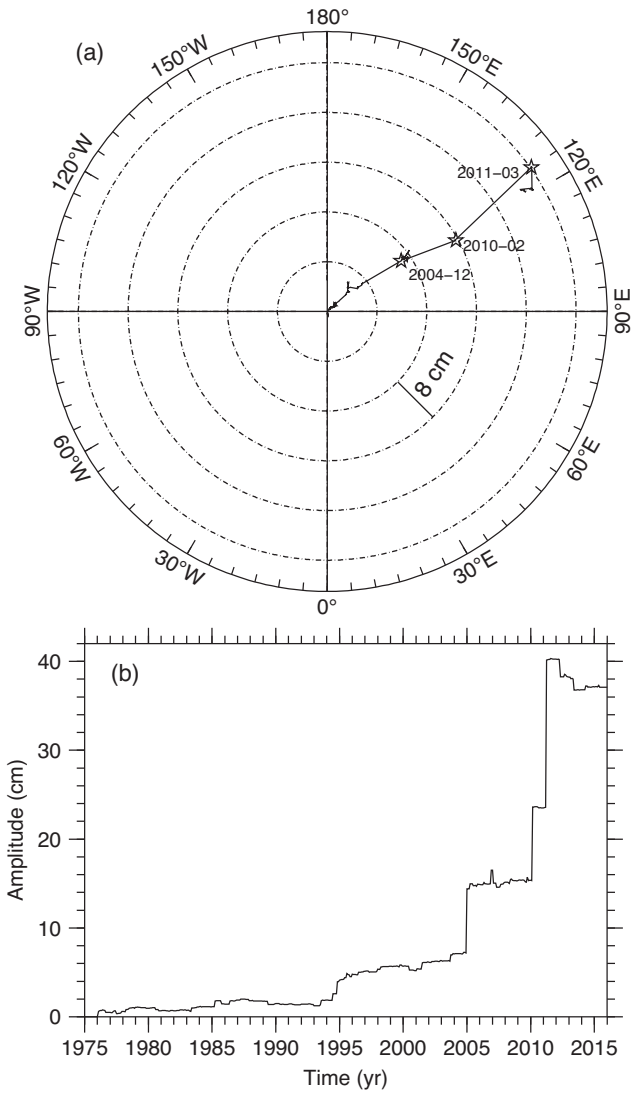

Figure 2. (a) Polar motion since 1976 to present obtained by implementing the CMT catalogue into the self-gravitating SNREI model based on PREM. The grey stars and labels indicate the time (year and month) at which occurred the December 2004 Sumatra, February 2010 Maule and March 2011 Tohoku earthquakes. (b) The amplitude of the accumulated polar shift since 1976 to present.

Table 1. Polar shift caused by the ten largest earthquakes since 1900.

Earthquake	M_w	Amplitude	Direction
May 1960 Chile	9.56	81.3 cm	113.2°E
December 2004 Sumatra	9.31	6.7 cm	125.5°E
March 1964 Alaska	9.18	27.5 cm	156.7°W
March 2011 Tohoku	9.08	16.8 cm	133.9°E
November 1952 Kamchatka	8.90	17.9 cm	151.6°E
February 2010 Maule	8.78	8.6 cm	110.5°E
February 1965 Rat Islands	8.70	4.2 cm	164.9°E
March 2005 Nias	8.61	0.7 cm	160.1°E
March 1957 Andreanof Islands	8.60	4.8 cm	174.0°E
May 1960 Valdivia	8.60	6.6 cm	104.9°E

Table 2. Trend of polar shift during different time intervals spanned by the CMT catalogue.

Period	$\partial_t M_s$	Rate	Direction
1976–2015	9.7×10^{21} N m yr^{-1}	9.4 mm yr^{-1}	121.0°E
1976–1993	2.9×10^{21} N m yr^{-1}	1.1 mm yr^{-1}	132.8°E
1994–2003	5.3×10^{21} N m yr^{-1}	5.2 mm yr^{-1}	126.7°E
2004–2015	24.2×10^{21} N m yr^{-1}	26.2 mm yr^{-1}	119.2°E

associated with the polar pattern is greater than the others by at least one order of magnitude.

We now give the analytical expression for the contribution to polar shift due to the polar pattern of the seismic perturbation

$$\delta\hat{\boldsymbol{m}} = S\, k_{2,0}^{\mathrm{D}}(r)\, \frac{M_0\ \sin(2\,\theta)\, \boldsymbol{s}(\varphi)}{a^3\, \mu(r)} \tag{7}$$

where θ and φ are the colatitude and longitude of the epicentre, μ is the shear modulus evaluated at the radius of the hypocentre, M_0 is the combination of the components of the seismic moment tensor given by eq. (A4a) (or by eq. (A7a) when interpreted in terms of the double couple, $M_0 = M_{\mathrm{s}} \sin(2\,\alpha) \sin(\gamma)$, with α and γ being the dip and rake angles), S is the following (negative) factor

$$S = -\frac{1}{1 - k_2^{\mathrm{T,E}}/k_2^{\mathrm{T,F}}}\, \frac{5\, M_{\mathrm{E}}\, a^2}{6\sqrt{3}\,(C - A)} \tag{8}$$

and $\boldsymbol{s}$ is the unit vector pointing towards the epicentral longitude

$$\boldsymbol{s}(\varphi) = \cos(\varphi)\, \boldsymbol{x}_1 + \sin(\varphi)\, \boldsymbol{x}_2. \tag{9}$$

In view of the fact that $k_{2,0}^{\mathrm{D}}$ is negative (see Fig. 1) and that the largest earthquakes are of the inverse type ($\sin(\gamma) > 0$), this main contribution displays the mean position of the rotation pole towards the same, φ, or opposite, $\psi + 180$, longitude of the epicentre depending whether the epicentre is in the northern (0–90°N and $\sin(2\,\theta) > 0$) or southern (0–90°S and $\sin(2\,\theta) < 0$) hemisphere. In view of eq. (7), the polar motion points towards the main subduction zones of the northern hemisphere (like the Sumatra-Java and Kamchatka/Kurils/Japan ones where the 2004 Sumatra and 2011 Tohoku earthquakes occurred) and in the opposite direction from the main subduction zones of the southern hemisphere (like the South America one where the 2010 Maule earthquake occurred), resulting in the general tendency of displacing the rotation pole towards about 120°E.

All the other contributions (from bipolar and quadrupolar pattern of the seismic perturbation or from intraplate and deep earthquakes) play a minor role in determining the amplitude and direction of polar motion, particularly that associated with the bipolar pattern of the seismic perturbation from intraplate earthquakes which is less than half millimetre (Supporting Information Figs S2b and e). The smallness of the latter can be understood by taking into account that intraplate seismicity represents only a small fraction of the global seismicity and that $k_{2,1}^{\mathrm{D}}$ is smaller than $k_{2,0}^{\mathrm{D}}$ by more than one order of magnitude at shallow depth (say, less than 50 km).

3 POLAR MOTION CAUSED BY INTERPLATE EARTHQUAKES SINCE THE BEGINNING OF THE PAST CENTURY

As discussed in the previous section, the CMT catalogue spans a too short time interval for establishing the trend of polar motion that we should expect from seismicity on the long term, namely on timescales larger than those characterizing short period fluctuations of seismicity. To mitigate the effect of the shortness, in time, of the CMT catalogue we thus perform the same simulation including also earthquakes from 1900 to 1975 relying on the ISC-GEM catalogue (Storchak *et al.* 2013).

Different from the CMT catalogue, the ISC-GEM catalogue only provides the hypocentre location (geographical coordinates and depth) and magnitude (seismic moment) for each earthquake. In light of this, we have to establish a procedure for assigning the earthquake mechanism (i.e. strike, dip and rake angles) to each seismic event before 1976, with the exception of the 1960 Chile and 1964 Alaska earthquakes, for which we rely on the specific studies of Kanamori (1970) and Kanamori & Cipar (1974) (see also Lambeck 1980). As we are going to detail and according to an approach similar to that adopted by O'Connell & Dziewonski (1976), we assign the earthquake mechanism according to the tectonic regime of the plate boundary closest to each earthquake, which in turn is obtained from information about plate kinematics at present-day and from the Anderson theory of faulting (Ranalli 1995).

This procedure makes sense only for interplate earthquakes and, thus, we shall leave out intraplate and deep earthquakes from the following simulation of polar motion. On the other hand, as already shown in Supporting Information Figs S1 and S2, the omission of intraplate or deep earthquakes does not affect our conclusions because their contribution to the polar motion is small compared to that from interplate earthquakes.

3.1 Earthquake mechanisms

We consider the NNR-MORVEL56 database of present-day plate kinematics (Argus *et al.* 2011) and the subdivision proposed by Bird (2003) of the plate boundaries into the sets of subduction zones, Γ_1, and oceanic, Γ_2, and continental, Γ_2, boundaries. We then obtain the unit vectors normal, $\hat{\boldsymbol{n}}$, and tangent, $\hat{\boldsymbol{t}}$, to the plate boundaries from the plate geometry. Particularly, we follow the convention that the cross product between the tangent and normal unit vectors points outwards from the Earth centre (i.e. $\hat{\boldsymbol{t}} \times \hat{\boldsymbol{n}} = \hat{\boldsymbol{r}}$), and we arbitrarily choose the direction of the tangent unit vector because the plate boundary only constrains the tangent line. From the Euler rotation poles, we also obtain the relative velocities between plates, $\boldsymbol{v}$, and we decompose it into the normal, v_{n}, and tangent, v_{t}, components

$$\boldsymbol{v} = v_{\mathrm{t}}\, \hat{\boldsymbol{t}} + v_{\mathrm{n}}\, \hat{\boldsymbol{n}} \tag{10}$$

with the convention that the normal component is positive for convergent boundaries ($v_{\mathrm{n}} > 0$) and negative for divergent boundaries ($v_{\mathrm{n}} < 0$).

Using this information from present-day plate kinematics, we may proceed in defining the procedure for assigning the earthquake mechanism to interplate earthquakes. We first assume that the line of strike of the fault system coincides with the plate boundaries. Then, according to the fact that seismicity accommodates the relative motion between plates (Davies & Brune 1971; Anderson 1975; Kagan 2002), we also assume that the along strike, $\partial_t u_1$, and along dip, $\partial_t u_2$, slip rates on the long term coincide with the tangential, v_{t}, and normal, v_{n}, components of the relative velocity between plates

$$\partial_t u_1 = v_{\mathrm{t}} \tag{11a}$$

$$\partial_t u_2 = v_{\mathrm{n}}. \tag{11b}$$

The rake angle, γ, is thus obtained in such a way that $\partial_t u_1 = v \cos(\gamma)$ and $\partial_t u_2 = v \sin(\gamma)$, with $v = \|\boldsymbol{v}\|$. This also allows us to infer the fault type: the fault is normal or inverse when $\gamma \in [225°, 315°]$ or $\gamma \in [45°, 135°]$, respectively, and strike-slip otherwise. Note that this is equivalent to infer the fault type by the comparison between the tangent and normal components of the relative velocity between plates. Particularly, when the tangent component is greater in absolute value than the normal component, $|v_{\mathrm{t}}| > |v_{\mathrm{n}}|$, the fault is strike-slip. Otherwise, $|v_{\mathrm{t}}| \leq |v_{\mathrm{n}}|$, the fault is normal for divergent plate boundaries, $v_{\mathrm{n}} < 0$, and inverse for convergent plate boundaries, $v_{\mathrm{n}} > 0$.

Finally, according to the Anderson theory of faulting and assuming a frictional coefficient of 0.75, we assign dip angles of 63°,

27° and 90° to normal, inverse and strike-slip faults, respectively (Ranalli 1995). We make an exception only for subduction zones, the dip angle of which is always fixed at 27°.

With this procedure we can fully characterize the earthquake mechanism, but for the strike angle which is determined only up to an angle of 180°, being inferred from the tangent to the plate boundary, the direction of which is chosen arbitrarily. Considering that the components (or combinations of components) of the seismic moment tensor, M_p ($p = -2, \ldots, 2$), eq. (A7), depend on the strike angle via the sine and cosine functions with argument $|p|\psi$, this ambiguity determines $M_{\pm1}$ except its sign while it does not affect M_0 and $M_{\pm2}$. In light of this, this ambiguity prevents us to determine only the contribution to polar motion associated with the bipolar pattern of the seismic perturbation. On the other hand, as already discussed in Section 2 and shown in Supporting Information Figs S1 and S2, this contribution is small and can be neglected. With this simplification, we do not need to resort to additional information in order to fully constrain the strike.

3.2 Results

Fig. 3 shows the polar motion obtained by implementing the ISC-GEM (since 1900 to 1975 and with the earthquake mechanism assigned according to the tectonic regime of the closest plate boundary of the NNR-MORVEL56 database) and CMT (since 1976 to present) catalogues. For this simulation, we take into account only interplate earthquakes (depth less than 50 km and within 220 km from plate boundaries).

The total polar shift accumulated since the beginning of the past century amounts to 190.0 cm and points towards 133.3°E. As reported in Table 3, we note that the average rate of polar shift is 16.5 mm yr^{-1} and that the rate from 1900 to 1975 (20.4 mm yr^{-1}) doubles that from 1976 to present (9.2 mm yr^{-1}). This larger rate of polar shift, compared to that obtained considering only the last four decades spanned by the CMT catalogue, is mainly attributable to the 1954 Kamchatka and 1960 Chile earthquakes which contribute with 17.9 cm/115.5 yr = 1.6 mm yr^{-1} and 81.3 cm/115.5 yr = 7.1 mm yr^{-1} towards 151.6°E and 113.2°E, respectively (see Table 1). Furthermore, the change of direction by about 12° from 121.0°E (from 1976 to present) to 133.3°E (from 1900 to present) is mainly due to the 1964 Alaska earthquake which displaces the mean position of the rotation pole by 27.5 cm towards 156.7°W. This direction, although almost perpendicular to the general trend towards 133.3°, is consistent with eq. (7) and results from the fact that the 1964 Alaska earthquake occurred at 147°W longitude in the northern hemisphere (at 61°N). As reported in Table 3, it is noteworthy that the seismic moment rates, $\partial_t M_s$, in the two time windows (from 1900 to 1975 and from 1976 to present) are roughly the same, about $8.3 \sim 8.4 \times 10^{21}$ N m yr^{-1}. This suggests that the long-term seismic moment rate at the global scale can be well estimated even using a little longer than one century (115.5 yr) of instrumental seismicity.

We note that our result differs significantly from that obtained by Chao & Gross (1987) on the basis of the calculations of polar shift due to the 30 largest earthquakes from 1900 to 1964 by O'Connell & Dziewonski (1976), about 13 cm yr^{-1} towards 148°E. During the same period, indeed, we estimate a trend of 2.3 cm yr^{-1} towards 136°E, that is smaller than that reported by Chao & Gross (1987) by about a factor of 5. This difference is attributable to the inaccuracy of the magnitude-seismic moment relation used by O'Connell & Dziewonski (1976) which overestimates the seismic moment of these 30 earthquakes by about one order of magnitude,

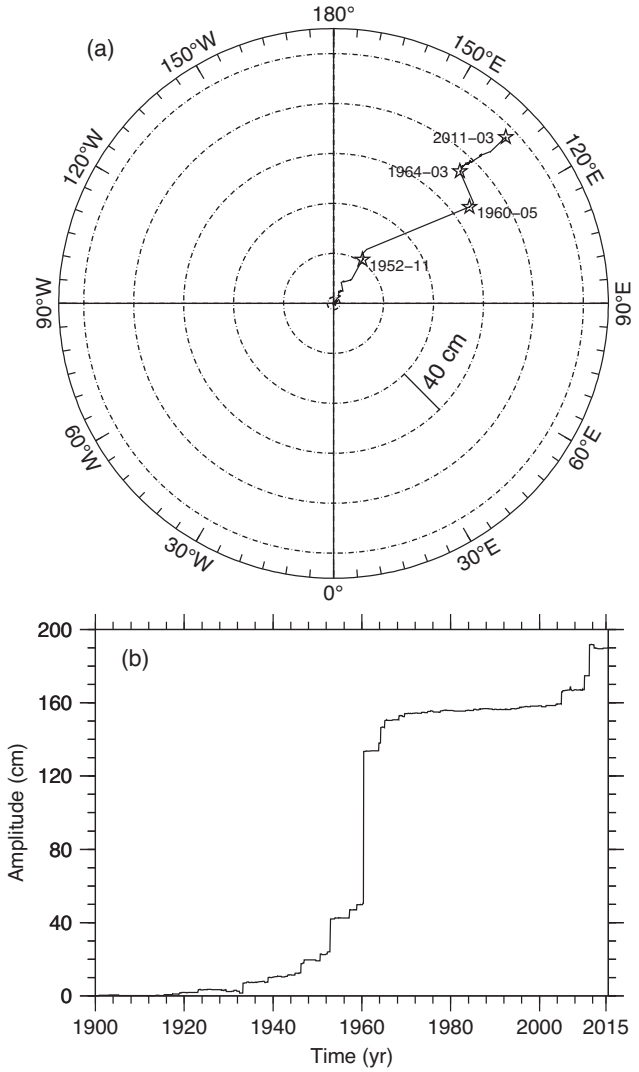

Figure 3. (a) Polar motion since 1900 to present obtained by implementing the interplate earthquakes of the CMT and ISC-GEM catalogues into the self-gravitating SNREI model based on PREM. The grey stars and labels indicate the time (year and month) at which occurred the November 1954 Kamchatka, May 1960 Chile, March 1964 Alaska and March 2011 Tohoku earthquakes. (b) The amplitude of the accumulated polar shift since 1900 to present.

in average. Indeed, according to the ISC-GEM catalogue, the total seismic moment of 28 earthquakes among the 30 earthquakes reported by O'Connell & Dziewonski (1976) (we do not consider the 14 September 1906 and 24 November 1914 earthquakes because they are in the supplementary ISC-GEM catalogue) is 5.2×10^{23} N m, while the magnitude-seismic moment relation used by O'Connell & Dziewonski (1976) yields a total seismic moment of 5.9×10^{24} N m.

This simulation over a little more than one century allows us to establish a more reliable estimate of the trend of polar motion caused by earthquakes than that based on the past four decades spanned by the CMT catalogue shown in Fig. 2, mainly because it includes a large number of giant earthquakes. In order to better understand how earthquakes with different magnitude contribute to polar motion and, particularly, whether the general tendency of displacing the mean position of the rotation pole towards 133°E is due to only megathrust earthquakes or to small earthquakes too, we show in

Table 3. Seismic moment rate and trend of polar motion caused by interplate earthquakes during different time intervals spanned by the ISC-GEM and CMT catalogues. The last row also reports the result obtained by implementing the global seismicity model (GSM) assuming a full seismic coupling, $\chi = 1$.

Period	$\partial_t M_s$	Rate	Direction
1900–2015.5	8.4×10^{21} N m yr^{-1}	16.5 mm yr^{-1}	133.3°E
1900–1975	8.4×10^{21} N m yr^{-1}	20.4 mm yr^{-1}	136.1°E
1976–2015.5	8.3×10^{21} N m yr^{-1}	9.2 mm yr^{-1}	121.0°E
1900–1964	9.1×10^{21} N m yr^{-1}	22.6 mm yr^{-1}	136.3°E
GSM	21.2×10^{21} N m yr^{-1}	20.0 mm yr^{-1}	112.5°E

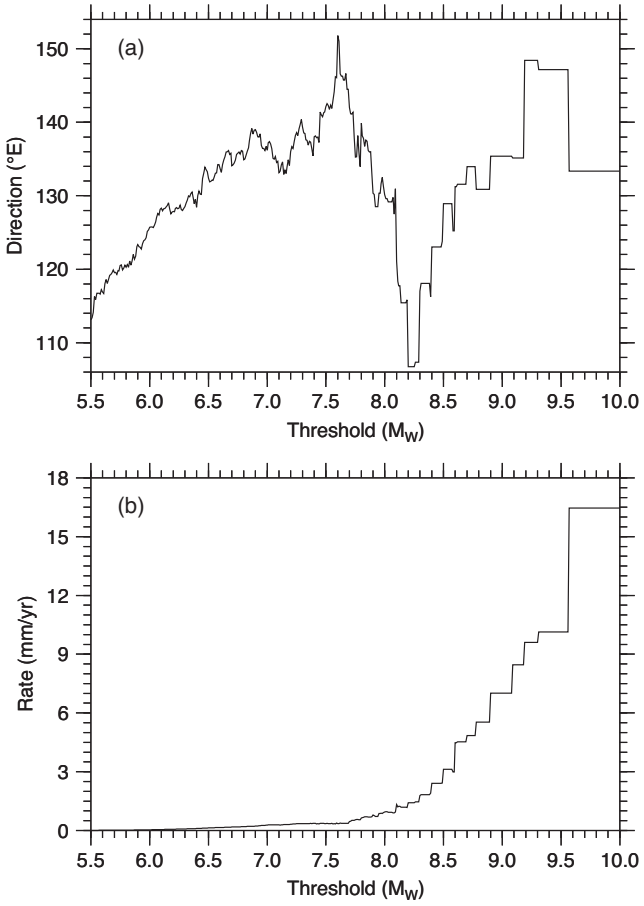

Figure 4. (a) Direction and (b) rate of the trend of polar motion since the beginning of the past century to present due to interplates earthquakes of the CMT and ISC-GEM catalogues with magnitude smaller than a threshold ranging from 5.5 to 10.0.

Fig. 4 the polar shift accumulated since the beginning of the past century due to earthquakes with magnitude smaller than a threshold ranging from 5.5 to 10.0. We note that, increasing the magnitude threshold from 5.5 to 7.6, the direction of polar motion varies from 113°E to 151°E, consistently with the general tendency towards 133°E. Nevertheless, earthquakes within this range of magnitude contribute to the rate of polar motion by less than half millimetre per year. Increasing further the threshold to 8.3, the direction changes to 107°E and, only including all giant earthquakes at subduction zones, reaches the final value of 133°. We note that the direction changes by about 13°, from 135°E to 148°E, including the 1964 Alaska earthquake (M_w 9.18). Then, it changes again to 147°E including the 2004 Sumatra earthquake (M_w 9.31) and to 133°E including

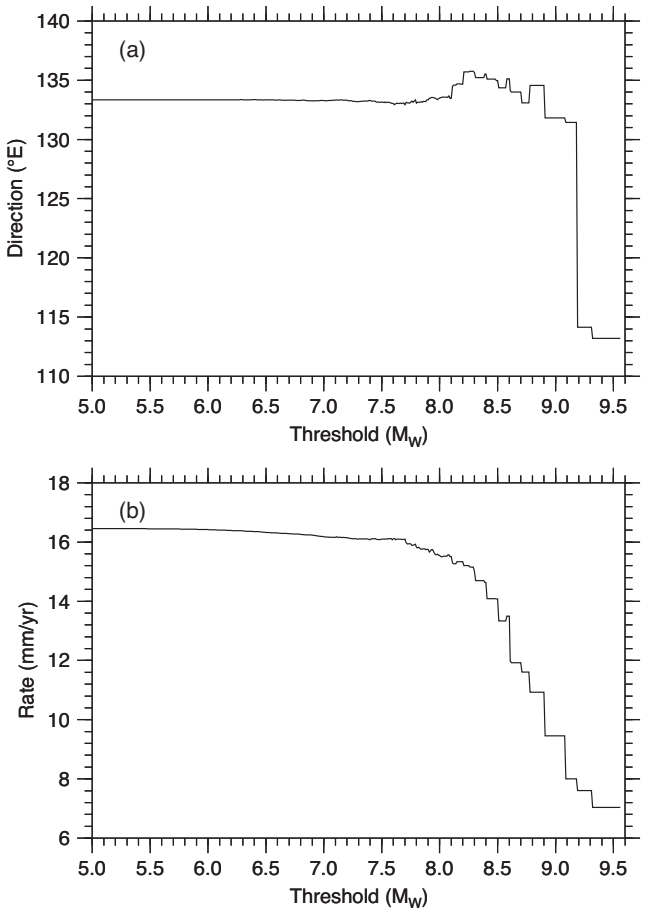

Figure 5. As Fig. 4 but considering earthquakes with magnitude greater (rather than smaller) than the threshold.

the 1960 Chile earthquake (M_w 9.56). In light of this analysis, we thus conclude that the available instrumental seismicity indicates a preferred direction of polar motion, subject to variations of the order of one or a few tens of degrees in response to individual megathrust earthquakes. This variability of the direction is the result of the fact that the available instrumental seismicity does not represent the average seismicity of all the subduction zones, otherwise individual megathrust earthquakes would not change the direction by more than ten degrees, like the 1964 Alaska event does.

A similar reasoning holds also for the estimate of the rate of polar motion. Indeed, even if the seismic moment rates at the global scale in the two time intervals (from 1900 to 1975 and from 1976 to present) almost coincide, the two estimates of the rate of polar motion differ by about a factor of 2. This significant difference can be explained considering that the amplitude of polar motion caused by seismic events is not simply proportional to the seismic moment, but it also depends on the epicentral colatitude and the earthquake mechanism. In this respect, the fact that the instrumental seismicity available still does not represent the average seismicity of all the subduction zones makes the related estimate of the rate of polar motion sensitive to individual megathrust earthquakes at specific subduction zones.

To better understand the sensitivity of the polar motion to earthquakes of different magnitude, we show in Fig. 5 also the polar shift accumulated since the beginning of the past century due to earthquakes with magnitude greater (rather than smaller as in Fig. 4) than a threshold ranging from 5 to 9.56 (that is the magnitude of

the 1960 Chile earthquake, the largest one). From this perspective, we note that earthquakes of magnitude smaller than 8 slightly affect the direction and rate of polar motion while earthquakes of magnitude smaller than 9 are responsible for changes of a few degrees in direction and for an increase from 8 mm yr^{-1} to 16 mm yr^{-1} in rate. Furthermore, we note that the 1964 Alaska earthquake (M_w 9.18) alone changes the direction of polar motion established by the 1960 Chile (M_w 9.56) and 2004 Sumatra (M_w 9.31) earthquakes of about 17°, from 114°E to 131°E.

4 THE GLOBAL SEISMICITY MODEL (GSM)

An alternative approach to establish the secular polar motion caused by interplate earthquakes can be achieved by further exploiting information about plate kinematics and combining it with the Anderson theory of faulting, as already done for assigning the earthquake mechanism to seismic events before 1976, and a few other simplifying assumptions that we are going to discuss. Our foremost goal will be to develop a GSM that describes seismicity along plate boundaries and that is independent from any earthquake catalogue. In this way we can overcome the issue of the limited information about the geographical distribution and recurrence of interplate earthquakes contained in the ISC-GEM and CMT catalogues.

First, we will use this GSM to simulate the trend of polar motion caused by interplate earthquakes and compare it with that obtained by implementing the earthquake catalogues in order to assess their mutual consistency. Finally, in Section 5, we will use it to account for interseismic deformations and to quantify, for the first time, their contribution to polar motion.

4.1 Fault system associated with plate boundaries

As discussed previously in Section 3, we will rely on the NNR-MORVEL56 database of plate kinematics in order to characterize the fault system associated with plate boundaries. Particularly, we assume that the line of strike of the fault system coincides with the plate boundaries and we introduce the along strike coordinate x by means of which we parametrize this line of strike worldwide. For the sake of simplicity, we also assume that the faults are homogeneous in depth and dip from the Earth surface down to a depth which only depends on the type of plate boundary: $Z_1 = 50$ km, $Z_2 = 10$ km and $Z_3 = 20$ km for subduction zones, Γ_1, and oceanic, Γ_2, and continental, Γ_3, boundaries, respectively. Within these assumptions, we can identify the infinitesimal surface elements of the fault system with the along strike coordinate, x, and depth, z. Furthermore, we note that the fault geometry (dip and strike angles) and the tangential displacement dislocation (or slip) shall be regarded as function of the only along strike coordinate x. Indeed, they depend only on the position along the plate boundaries since the faults are assumed to be homogeneous in depth.

To each infinitesimal segment of the plate boundaries we then assign the fault geometry (dip and strike) according to the earthquake mechanism inferred with the same procedure described in Section 3.1. Nevertheless, using only information about plate kinematics at the Earth surface, we cannot establish whether the faults dip to the left or to the right of the plate boundaries and this prevents us to define the surface of the fault system in depth. This issue is an additional counterpart of the fact the strike angle is determined up to 180° being inferred from the tangent to the plate boundary, the direction of which is chosen arbitrarily. In order to overcome the latter complexity, we decide to neglect the spatial extent of the faults perpendicularly to the line of strike, that does not exceed a few hundreds km even for subduction zones. This is correct because this extension is smaller by about two orders of magnitude than the wavelength of 20 000 km involved in the rotational dynamics of the Earth and means that we locate every infinitesimal surface element of the fault system just below the plate boundary (without altering its depth and geometry). Then, similar to the fault geometry, the angular coordinates of the infinitesimal surface elements depend only on the along strike coordinate, even if the faults are not vertical. After this simplification, the ambiguity about the strike angle refers solely to the geometry (i.e. the strike angle itself) of the infinitesimal surface elements, but it does not concern their geographic position.

In the end, since the relative motion between plates is accommodated by slip over the fault system associated with the plate boundaries, the long-term slip rate over this fault system is obtained from the relative velocity between plates, as in eq. (11). This means that, in addition to the rake angle and the fault type, the relative velocity between plates is now used to estimate the slip rate. In this respect, this slip rate takes into account both seismic (stick-slip earthquakes) and aseismic (slow earthquakes and fault creep) contributions and, in order to consider only the seismic one, in place of eq. (11), we shall set

$$\partial_t u_1 = \chi\, v_t \tag{12a}$$

$$\partial_t u_2 = \chi\, v_n \tag{12b}$$

where χ is the seismic coupling coefficient. This coefficient describes the amount of the relative motion between plate that is accommodated by seismic slip (Kagan 2002).

The seismic coupling coefficient is still a not well constrained quantity and may vary from one fault to another, as well as on a fault itself (Bird & Kagan 2004; Kagan 2014). For the sake of simplicity, hereinafter we decide to keep the seismic coupling coefficient constant over the whole fault system and, according to the seismic moment conservation principle proposed by Kagan (2002), we estimate it from the comparison of the seismic, $\partial_t M_s$, and tectonic, $\partial_t \mathrm{M_T}$, moment rates at the global scale

$$\partial_t M_s = \chi\, \partial_t \mathrm{M_T} \tag{13}$$

with the tectonic moment rate defined as follows

$$\partial_t \mathrm{M_T} = \int_{\mathcal{S}} \mu\, v\, \mathrm{d}S. \tag{14}$$

Here $\mathcal{S}$ is the surface of the fault system and dS is the area of the infinitesimal surface element. Within the assumption that we made in defining the GSM, the implementation of eq. (14) is quite straightforward and yields a tectonic moment rate of 21.2×10^{22} N m yr^{-1} that is about twice the seismic moment rate estimated from 1900 to present on the basis of the CMT and ISC-GEM catalogues, 8.4×10^{21} N m yr^{-1} . In view of eq. (13), this implies a seismic coupling coefficient of 0.4, consistent with other previous estimates, particularly at subduction zones (Bird & Kagan 2004; Kagan & Jackson 2013; Kagan 2014).

4.2 Mathematical formulation

Let us now discuss how to implement the GSM into self-gravitating SNREI Earth model and, particularly, take advantage of the assumptions that we made in its definition to obtain compact expressions for simulating the secular polar motion caused by interplate earthquakes.

As discussed in Cambiotti & Sabadini (2015), the perturbation of the Earth inertia caused by tangential displacement dislocations over a fault system with surface $\mathcal{S}$ reads

$$\Delta \mathrm{I}_{i3} = \frac{M_\mathrm{E}}{a} \sum_{p=0}^{2} \sum_{j=1}^{2} \int_{\mathcal{S}} k^\mathrm{D}_{2,p}(r)\, B^p_{i,j}\, u_j \,\mathrm{d}S \qquad \forall\, i = 1, 2, \tag{15}$$

where u_1 and u_2 are the components of the slip along the strike and dip, and $B^p_{i,j}$ ($i = 1, 2, j = 1, 2, p = 0, 1, 2$) are given by

$$B^p_{1,j} = -\sqrt{\frac{5}{3}}\, \frac{D^p_j\, F^p_{2-1} + D^{-p}_j\, F^{-p}_{2-1}}{1 + \delta_{p,0}} \tag{16a}$$

$$B^p_{2,j} = -\sqrt{\frac{5}{3}}\, \frac{D^p_j\, F^p_{21} + D^{-p}_j\, F^{-p}_{21}}{1 + \delta_{p,0}}. \tag{16b}$$

Here, $\delta_{i,j}$ is the Kronecker delta, D^p_j ($j = 1, 2; p = -2, \ldots, 2$) are factors which depend on the geometry of the infinitesimal surface element (strike, ψ, and dip, α, angles)

$$D^0_1 = 0 \tag{17a}$$

$$D^{-1}_1 = -\cos(\psi)\, \cos(\alpha) \tag{17b}$$

$$D^1_1 = \sin(\psi)\, \cos(\alpha) \tag{17c}$$

$$D^{-2}_1 = -\sin(2\,\psi)\, \sin(\alpha) \tag{17d}$$

$$D^2_1 = -\cos(2\,\psi)\, \sin(\alpha) \tag{17e}$$

$$D^0_2 = \sin(2\,\alpha) \tag{17f}$$

$$D^{-1}_2 = -\sin(\psi)\, \cos(2\,\alpha) \tag{17g}$$

$$D^1_2 = -\cos(\psi)\, \cos(2\,\alpha) \tag{17h}$$

$$D^{-2}_2 = \frac{1}{2} \sin(2\,\psi)\, \sin(2\,\alpha) \tag{17i}$$

$$D^2_2 = -\frac{1}{2} \cos(2\,\psi)\, \sin(2\,\alpha) \tag{17j}$$

and F^p_{2m} ($m = \pm 1; p = -2, \ldots, 2$) are functions of the angular coordinates (colatitude, θ, and longitude, φ) of the infinitesimal surface element

$$F^{-2}_{2-1} = -\frac{1}{2} \sin(2\,\theta) \cos(\varphi) \tag{18a}$$

$$F^{-1}_{2-1} = \cos(2\,\theta) \cos(\varphi) \tag{18b}$$

$$F^0_{2-1} = \frac{\sqrt{3}}{2} \sin(2\,\theta) \cos(\varphi) \tag{18c}$$

$$F^1_{2-1} = -\cos(\theta) \sin(\varphi) \tag{18d}$$

$$F^2_{2-1} = \sin(\theta) \sin(\varphi) \tag{18e}$$

$$F^{-2}_{21} = -\frac{1}{2} \sin(2\,\theta) \sin(\varphi) \tag{18f}$$

$$F^{-1}_{21} = \cos(2\,\theta) \sin(\varphi) \tag{18g}$$

$$F^0_{21} = \frac{\sqrt{3}}{2} \sin(2\,\theta) \sin(\varphi) \tag{18h}$$

$$F^1_{21} = \cos(\theta) \cos(\varphi) \tag{18i}$$

$$F^2_{21} = -\sin(\theta) \cos(\varphi). \tag{18j}$$

Since plate kinematics provides the long-term slip rates, eq. (32), rather than the exact time evolution of slip, from now on we shall consider only the trend of polar motion. In other words, we consider the time derivative of the direction cosines given by eq. (3),

$$\partial_t m_i = \frac{1}{1 - k^{\mathrm{T,E}}_2 / k^{\mathrm{T,F}}_2}\, \frac{\partial_t \Delta I_{i3}}{C - A}, \tag{19}$$

where the rate of change of the Earth inertia, $\partial_t \Delta I_{i3}$ is obtained by substituting the slip with the slip rates into eq. (15)

$$\partial_t \Delta \mathrm{I}_{i3} = \frac{M_\mathrm{E}}{a} \sum_{p=0}^{2} \sum_{j=1}^{2} \int_{\mathcal{S}} k^\mathrm{D}_{2,p}(r)\, B^p_{i,j}\, \partial_t u_j \,\mathrm{d}S. \tag{20}$$

This is motivated by the fact that the fault system associated with plate boundaries can be considered fixed in space on timescales smaller than geological times, say one million years. In fact, assuming a motion of plate boundaries of $10\,\mathrm{cm\,yr^{-1}}$, the fault surface is displaced by about 100 km on this timescale and this is negligible once compared to the wavelength of 20 000 km involved by the rotational dynamics of the Earth.

In view of the simplification adopted in the definition of the GSM, the dip and strike angles, the slip rate and the colatitude and longitude of the infinitesimal surface element only depend on the along strike coordinate x. In light of this, the integrand in the right-hand side of eq. (20) depends on depth only via the seismic Love numbers and, then, we can write

$$\partial_t \Delta \mathrm{I}_{i3} = \frac{M_\mathrm{E}}{a} \sum_{p=0}^{2} \sum_{j=1}^{2} \int_{\Gamma} \frac{Z(x)\, \bar{k}^\mathrm{D}_{2,p}(Z(x))\, B^p_{i,j}(x)\, \partial_t u_j(x)}{\sin(\alpha(x))} \,\mathrm{d}x. \tag{21}$$

Here, $\Gamma = \Gamma_1 \cup \Gamma_2 \cup \Gamma_3$ is the set of the lines of strike of the fault system, $Z(x)$ is the depth of the seismogenic zone at the along strike coordinate x, and $\bar{k}^\mathrm{D}_{2,p}$ are the seismic Love numbers averaged over the depth of the seismogenic zone

$$\bar{k}^\mathrm{D}_{2,p}(Z) = \frac{1}{Z} \int_0^Z k^\mathrm{D}_{2,p}(a - z) \,\mathrm{d}z. \tag{22}$$

Note that we have made use of $\mathrm{d}S = \mathrm{d}x\, \mathrm{d}z / \sin(\alpha)$.

In the end, in view of the assumption that the depth of the seismogenic zone is constant along plate boundaries of a given type, eq. (21) further reduces to

$$\partial_t \Delta \mathrm{I}_{i3} = M_\mathrm{E}\, a^2 \sum_{p=0}^{2} \sum_{k=1}^{3} \bar{k}^\mathrm{D}_{2,p}(Z_k)\, A^p_{i,k}, \tag{23}$$

where $A^p_{i,k}$ ($i = 1, 2; k = 1, 2; p = 0, 1, 2$) are defined as follows

$$A^p_{i,k} = \frac{Z_k}{a^3} \sum_{j=1}^{2} \int_{\Gamma_k} \frac{B^p_{i,j}(x)\, \partial_t u_j(x)}{\sin(\alpha(x))} \,\mathrm{d}x. \tag{24}$$

Here the index k is used to indicate the type of plate boundary: $k = 1$, 2 and 3 for subduction zones, and oceanic and continental boundaries, respectively.

From eq. (17), we note that the factors D^p_j depend on the strike angle via sine and cosine functions with argument $|p|\zeta$. This means that the ambiguity about the strike angle (which is determined up to 180° from plate kinematics as discussed in Section 3) does not affect the factors $B^0_{i,j}$ and $B^2_{i,j}$ and, then, the GSM can be used for calculating the factors $A^0_{i,k}$ and $A^2_{i,k}$ associated with polar and quadrupolar patterns of the seismic perturbation. Differently, this ambiguity makes the factor $B^1_{i,j}$ determined up to the sign and, then, the factors $A^1_{i,j}$ associated with the bipolar pattern of the seismic perturbations cannot be calculated. This issue is irrelevant for strike-slip faults because, within the framework of the GSM, they are vertical faults (dip angles of 90°) and, thus, the contribution associated with the bipolar pattern is zero by definition, eq. (17). For normal and inverse faults, instead, the ambiguity about the strike angle remains and their contribution associated with the bipolar pattern cannot be quantified. However, as discussed in Section 2.2 and shown in Supporting Information Fig. S1 for the case of the polar motion obtained using the CMT catalogue, this contribution can be neglected because it is smaller by about one order of magnitude than the total amount.

4.3 Results

According to the framework presented above and using eqs (19) and (23), we simulate the secular polar motion by implementing the GSM based on the NNR-MORVEL56 database of plate kinematics. This simulation is independent from any earthquake catalogue and represents the secular polar motion that we expect from interplate seismicity on the basis of present-day plate kinematics. We do not account yet for interseismic deformations, which will be discussed below, and we keep the seismic coupling coefficient, χ, as a free parameter because the simulated rate of polar shift is simply proportional to it and the direction does not depend on this parameter. This simple dependence on the seismic coupling coefficient results from the fact that we have assumed that the slip rate over the whole fault system scales linearly versus this coefficient, eq. (32).

Assuming that the relative motion between plates is fully accommodated by seismic slip (i.e. a full seismic coupling with $\chi = 1$), the trend of polar motion obtained from the GSM yields 20.0 mm yr^{-1} towards 112.5°E (see Table 3). Considering only the contribution due to seismic slip as estimated by the seismic moment conservation principle (i.e. a partial seismic coupling with $\chi = 0.4$), the rate of polar motion decrease to 8.0 mm yr^{-1} while the direction is not altered. These trends are comparable, both in amplitude and direction, with that obtained by implementing the ISC-GEM and CMT catalogues since the beginning of the past century, 16.5 mm yr^{-1} towards 133.3°E. Nevertheless, the direction differs by about 20°, and the rate of polar motion is greater by about 20 per cent for $\chi = 1$ and smaller by about 50 per cent for $\chi = 0.4$. Although our GSM can still be improved in order to describe even better the long-term average seismicity along plate boundaries, these differences do not necessarily indicate serious inaccuracies related to some of the simplifying assumptions that we made in defining it. Rather, as already argued in Section 3, some differences between the long-term trend of polar motion and that obtained from the earthquake catalogues must be expected because the available instrumental seismicity, spanning a little longer than one century, does not represent the average seismicity of all subduction zones.

5 RESIDUAL POLAR MOTION CAUSED BY COSEISMIC AND INTERSEISMIC DEFORMATIONS

The simulations discussed in the previous sections, as well as in the previous literature, imply that seismicity yields a secular polar motion. Although this conclusion is theoretically correct on the basis of the previous hypotheses, what we expect to observe in EOP time-series on timescales of decades or centuries is not such a secular contribution because it is necessarily intermingled with that associated with interseismic deformations, as well as with all the other contributions coming from the different processes characterizing the seismic cycle (slow earthquakes, fault creep, viscoelastic and poroelastic postseismic deformations, etc.).

In this study, we consider the simplest sketch of the seismic cycle within the framework of an elastic Earth, leaving out additional effects due to viscoelasticity and poroelasticity. Furthermore, as already done in the definition of the GSM, we discriminate the slip over the fault system associated with the plate boundaries into contributions from seismic and aseismic processes. The seismic slip accounts only for stick-slip earthquakes. The aseismic slip, instead, is not necessarily a steady fault creep. Recent advances in instrumentation and measurements have allowed researchers in the last decade to change our previous thinking about the responses of the Earth. Microseismicity and slow earthquake tremors (Obara 2002; Beroza & Ide 2011) in non-volcanic ductile environments reveal a much richer role of crustal and mantle rheology than a simple dash-pot, absorbing the seismic energy transferred from the brittle crust. Tremor in San Andreas below the brittle faults is attributed to triggered slow creep as a possible mechanism for delayed dynamic triggering of tremor and earthquakes (Shelly *et al.* 2011). We thus regard any departure from the average aseismic slip rates as the results of slow earthquakes and, in a time interval $[0, T]$, we formally decompose the time history of the slip, u, as follows

$$u(t) = u_e(t) + u_s(t) + v_c\, t \qquad 0 \le t \le T \tag{25}$$

where u_e and u_s are the contributions from stick-slip earthquakes and the departure of the aseismic slip from the steady fault creep, respectively, and $v_c\, t$ is the steady fault creep. By definition, u_e is a step-like function describing the sudden slips of every earthquake and u_s is a continuous function, the average of which yields zero on the long term (i.e. for $T \to \infty$)

$$\lim_{T\to\infty} \int_0^T u_s(t)\, \mathrm{d}t = 0. \tag{26}$$

According to Savage & Burford (1973) and Savage (1983), the steady relative motion between plate is responsible for static deformations, like the peculiar topography at subduction zones, but it does not contribute to observable changes through time. Within this scheme the contribution to slip from the steady fault creep, $v_c\, t$ in eq. (25), does not yield any time-dependent perturbation of the Earth inertia and, thus, must be omitted in simulations of polar motion. Furthermore, in order that the steady relative motion between plate results into only static deformations, it is necessary to take into account interseismic deformations associated with the locking phase of the fault system among the seismic events. The most effective way to account for this contribution consists in adding a supplemental term to eq. (25) that describes a constant slip rate that is opposite to the seismic slip on the long term (Savage & Burford 1973; Savage 1983; Segall 2010) and that we denote with v_i

$$\lim_{T\to\infty} \left(-\frac{u_e(T)}{T} \right) = v_i \tag{27}$$

Note that, since plate motion is accommodated by both seismic and aseismic slip, we have

$$v = v_c - v_i \tag{28}$$

where v is the relative velocity between plates, or, equivalently,

$$v_c = (1 - \chi)\, v \tag{29}$$

$$v_i = -\chi\, v, \tag{30}$$

where χ is the seismic coupling coefficient. In light of these considerations, the terms of the slip that are expected to contribute to observable changes through time read

$$u(t) = u_e(t) + v_i\, t + u_s(t) \qquad 0 \le t \le T \tag{31}$$

where the second term in the right-hand side, $v_i\, t$, accounts for interseismic deformations.

In view of eq. (27), stick-slip earthquakes and interseismic deformations associated with the locking phase of the fault system among seismic events, taken together, compensate each other on the long term and, thus, they do not yield any secular polar motion. On the short term, however, we must expect a residual polar motion because the geographical distribution and recurrence of interplate earthquakes differ from those corresponding to the constant slip rate which accounts for interseismic deformations and is distributed over the whole fault system. The simplest way of modelling this residual polar motion consists in assuming that interseismic deformations are responsible for a trend that is opposite to that due to stick-slip earthquakes. Considering the trend of polar motion due to interplate earthquakes since the beginning of the past century (see Fig. 3 and Table 3), we thus can assume that interseismic deformations yield a steady polar motion of the same rate, 16.5 mm yr^{-1}, but pointing towards the opposite direction, 46.7°W. Fig. 6 shows the residual polar motion obtained according to this scheme. By definition, the rotation axis is exactly at the north pole at 1900 and at present. At intermediate times, instead, it departs from the north pole by at most 65.7 cm and remains close to the 47°W and 133°E meridians. Furthermore, we note that interseismic deformations dominate over coseismic deformations before the 1960 Chile and 1964 Alaska earthquakes and this makes the rotation pole moving towards about 47°W. Then, these two giant earthquakes displace the rotation pole almost in the opposite direction and, afterwards, interseismic deformations dominate again, bringing back the rotation pole at the north pole.

In view of eq. (26), we expect that departures of the aseismic slip from the steady fault creep yield a similar residual polar motion around the north pole, although smoothed in time. This additional contribution to polar motion cannot be modelled mainly because slow earthquakes can be hardly detected all around the world in a systematic way, differently from stick-slip earthquakes. In light of this, we will not further discuss the case of slow earthquakes, although we recognize that their contribution can be comparable with that from coseismic and interseismic deformations.

5.1 Results

Fig. 6 has been shown mainly with the intent of providing a first example and of better explaining what the residual polar motion due to coseismic and interseismic deformations should be on the short term. Nevertheless, the assumption that coseismic and interseismic deformations cancel each other over a time interval of about century hardly applies to realistic situation.

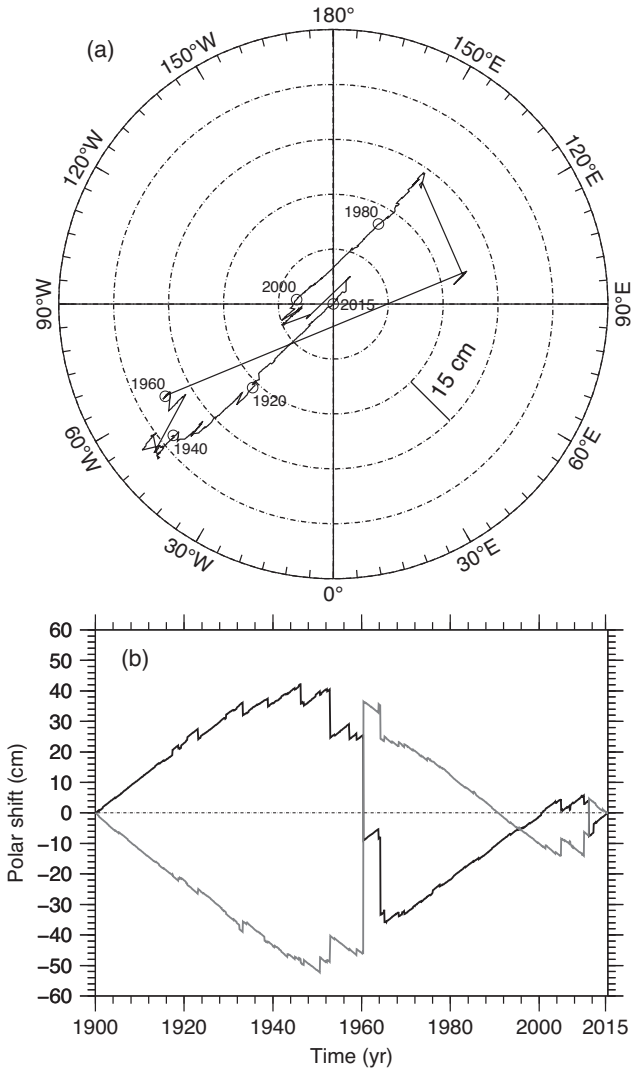

Figure 6. (a) Polar motion since 1900 to present due to both coseismic and interseismic deformations. The contribution from coseismic deformations is obtained by implementing the interplate earthquakes of the CMT and ISC-GEM catalogues. The contribution from interseismic deformation, instead, has been assumed to be a steady trend opposite to that from coseismic deformations, that is, 16.5 mm yr^{-1} towards 46.7°W. The circles and labels indicate the time (in year). (b) The components of the accumulated polar shift along the 0° and 90°E longitudes (black and grey lines, respectively).

A more realistic simulation of the residual polar motion since the beginning of the past century to present can be achieved by exploiting further the GSM. Particularly, in view of eq. (30), the GSM can be adapted to simulate interseismic deformations by setting the along strike and along dip slip rates as follows

$$\partial_t u_1 = -\chi\, v_{\mathrm{t}} \tag{32a}$$

$$\partial_t u_2 = -\chi\, v_{\mathrm{n}}. \tag{32b}$$

In this way, the contribution from interseismic deformations is not set *ad hoc* to respect conditions that should holds only on the long term, and not on the timescale of a century.

According to this scheme and recalling the results presented in Section 4, interseismic deformations yield a steady polar motion towards 67.5°W at rate of 8 mm yr^{-1} in the case of a partial seismic coupling, as it has been inferred from the seismic moment

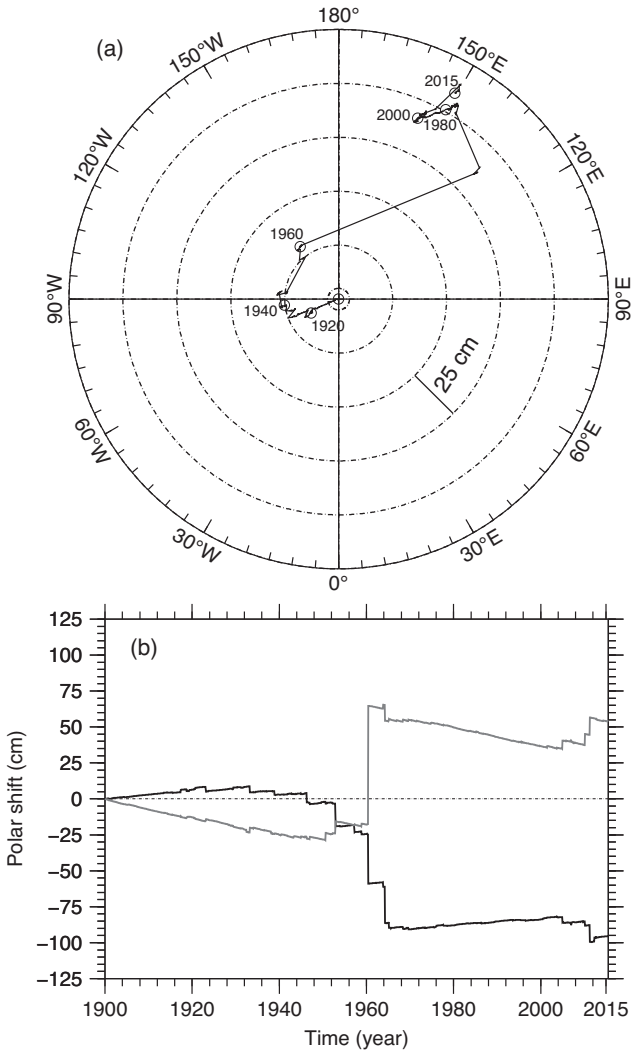

Figure 7. (a) Polar motion since 1900 to present due to both coseismic and interseismic deformations obtained by implementing the interplate earthquakes of the CMT and ISC-GEM catalogues and the GSM into the self-gravitating SNREI model based on PREM. For this simulation, we used the seismic coupling coefficient estimated on the basis of the seismic moment conservation principle, $\chi = 0.40$, as discussed in Section 4. The circles and labels indicate the time (in year). (b) The components of the accumulated polar shift along the 0° and 90°E longitudes (black and grey lines, respectively).

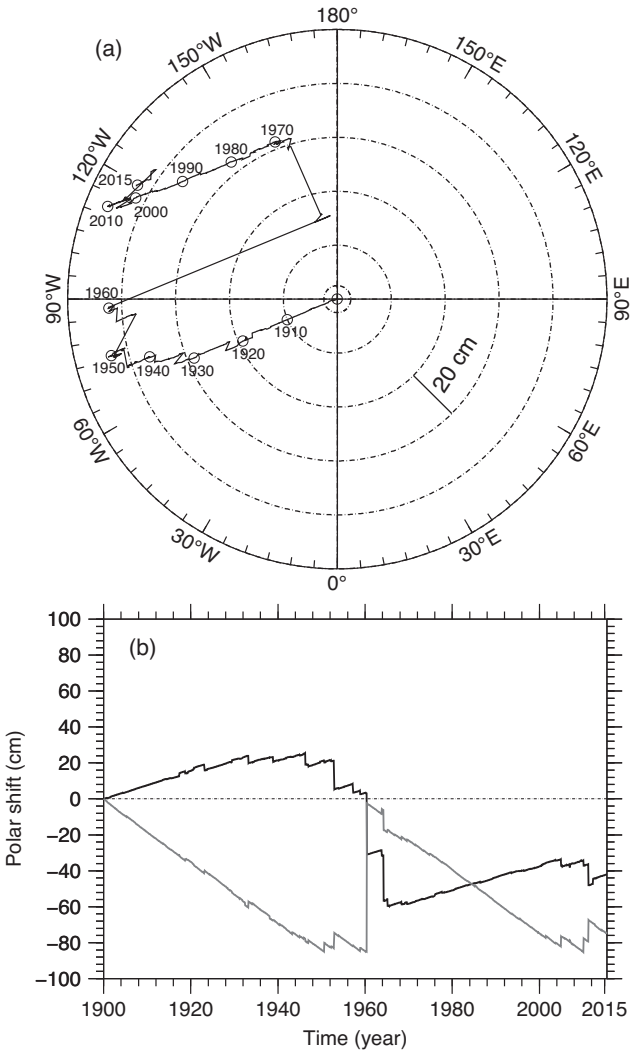

Figure 8. The same as Fig. 7, but assuming a full seismic coupling, $\chi = 1$.

conservation principle ($\chi = 0.4$), and at the rate of 20 mm yr^{-1} in the case of a full seismic coupling ($\chi = 1$). Figs 7 and 8 show the residual polar motion for these two cases. Differently from the example shown in Fig. 6, the rotation pole does not come back to the north pole at present but it gains a net shift of 109.6 cm towards 150.5°E for $\chi = 0.4$ and of 85.7 cm towards 119.3°W for $\chi = 1$. These net gains result from the vectorial sum of the trends of polar motion due to coseismic and interseismic deformations that do not cancel each other exactly. Indeed, as already noticed, the past century of seismicity is still affected by individual megathrust earthquakes and, then, it does not represent the average seismicity of all subduction zones. On the contrary, interseismic deformations, evolving linearly with time and being distributed over the whole fault system associated with plate boundaries according to the relative motion between plates, are already representative of their average on the long term. In other words, as one should expect and as implied by the assumption made in defining the GSM, the trend due to interseismic deformations is not sensitive to the time interval over which it is estimated, that is, it is (almost) the same both on the long and short term. Only at geological timescales, during phase of plate tectonic reorganizations, this contribution thus changes.

6 CONCLUSIONS

First, we have simulated the secular polar motion caused by global seismicity updated to the last release of the CMT catalogue (from 1976 to present) and extended to the beginning of the past century assigning the earthquake mechanism at seismic events before 1976 contained in the ISC-GEM catalogue (from 1900 to present) on the basis of the tectonic regime inferred from the NNR-MORVEL56 database of plate kinematics. Different from previous works on this subject (e.g. O'Connell & Dziewonski 1976; Chao & Gross 1987; Chao *et al.* 1996; Soldati *et al.* 2001; Zhou *et al.* 2013), we have taken into account the longest period available of instrumental seismicity in order to mitigate, as much as possible, the impact of the shortness, in time, of the earthquake catalogue on our conclusions about this contribution to polar motion.

Despite this effort, the little longer than one century of instrumental seismicity does not represent yet the average seismicity that

we should expect on the long term at least at the main subduction zones. Indeed, the estimated trend of polar motion (16.5 mm yr^{-1} towards 133.3°E) is still sensitive to individual megathrust earthquakes. Particularly, the 1960 Chile and 1964 Alaska earthquakes contribute to the average rate and direction by about 6 ∼ 7 mm yr^{-1} and 13 ∼ 14°, respectively (Figs 3 and 4).

In order to further investigate this issue, we have developed a GSM that is independent from any earthquake catalogue and that describes the average seismicity along plate boundaries on the long term. This has been made possible by combining information about present-day plate kinematics with the Anderson theory of faulting and a few other assumptions. Within this framework, we have obtained a secular polar motion of 8 mm yr^{-1} towards 112.5°E that is comparable with that estimated using the CMT and ISC-GEM catalogues, although smaller by about a factor of 2 in amplitude and differing by about 20° in direction. This simulation assumes a partial seismic coupling that we have estimated according to the seismic moment conservation principle (i.e. about the 40 per cent of the relative motion between plates is accommodated by seismic slip over the whole fault system associated with the plate boundaries while the remaining 60 per cent by aseismic slip). In the case of a full seismic coupling, instead, the rate of the polar motion increases to 20 mm yr^{-1} while the direction towards 112.5°E is not altered.

Our analysis shows that seismicity cannot be responsible for secular polar motion by arguing that interseismic deformations are expected to compensate it. Indeed, according to Savage & Burford (1973) and Savage (1983), coseismic and interseismic deformations, in first approximation and on average, cancel out each other leaving only steady block motion between adjacent plates. In other words, we have reconciled the idea of a secular polar motion caused by earthquakes with our simplest understanding of the seismic cycle. This is important because what we shall simulate and, hopefully, observe in EOP time-series on timescales of decades or centuries is the polar motions caused by both coseismic and interseismic deformations, being necessarily intermingled. The contribution from the only coseismic deformations, instead, can be discriminated by determining breaks in the prograde circular motion of the rotation pole corresponding to sudden excitations associated with large seismic events (Smylie & Zuberi 2009; Smylie *et al.* 2015) and this means to consider only one earthquake at time, rather than the cumulative effect of the earthquake sequence.

In this perspective, we have redefined our GSM in order to model the contribution to polar motion from interseismic deformations and, combining this contribution with that from coseismic deformations obtained using the CMT and ISC-GEM catalogues, we have simulated the residual polar motion resulting from these two opposite processes since the beginning of the past century. As expected, coseismic and interseismic deformations, taken together, make the rotation pole wander around the north pole with maximum polar excursions of about 1 m. Particularly, the rotation pole moves towards about Newfoundland when interseismic deformations dominate over coseismic ones (i.e. during phases of low seismicity or, equivalently, when most of the fault system associated with plate boundaries is locked). In the other case, when megathrust earthquakes occur, the rotation pole is suddenly shifted in the almost opposite direction, towards about 133°E. Furthermore, due to the fact that interseismic and coseismic deformations do not exactly compensate each other on the timescales of decades or centuries, the rotation pole gains, at present and with respect to its initial position at the north pole at 1900, a net shift of 110 cm towards 151°E and of 86 cm towards 119°W in the cases of partial and full seismic coupling, respectively. This net shift, however, is only temporary and should not be confused with a secular polar motion on the long term. Extending these simulations at later times, indeed, will make the rotation pole still wandering around the north pole, with maximum polar excursions determined by the trade-off between coseismic and interseismic deformations.

ACKNOWLEDGEMENTS

This research was partially supported by the CAS/CAFEA international partnership program for creative research teams (No. KZZD-EW-TZ-19) and the grant to David Yuen from Geochemistry and Geophysics Program of National Science Foundation. We thank Duncan Agnew for his constructive comments, in particular for suggesting that we consider interseismic deformations.

REFERENCES

Anderson, D., 1975. Accelerated plate tectonics, *Science,* **187,** 1077–1079.

Argus, D.F., Gordon, R.G. & DeMets, C., 2011. Geologically current motion of 56 plates relative to the no-net-rotation reference frame, *Geochem. Geophys. Geosyst.,* **12,** Q11001, doi:10.1029/2011GC003751.

Beroza, G. & Ide, S., 2011. Slow earthquakes and nonvolcanic tremor, *Annu. Rev. Earth Planet. Sci.,* **39,** 271–296.

Bird, P., 2003. An updated digital model of plate boundaries, *Geochem. Geophys. Geosyst.,* **4,** 1027, doi:10.1029/2001GC000252.

Bird, P. & Kagan, Y., 2004. Plate-tectonic analysis of shallow seismicity: Apparent boundary width, beta, corner magnitude, coupled lithosphere thickness, and coupling in seven tectonic settings, *Bull. seism. Soc. Am.,* **94,** 2380–2399.

Cambiotti, G. & Sabadini, R., 2013. Gravitational seismology retrieving centroid moment tensor solution of the 2011 Tohoku earthquake, *J. geophys. Res.,* **118,** 183–194.

Cambiotti, G. & Sabadini, R., 2015. On the seismic perturbation due to a fault system: its evaluation beyond the epicentral reference frame, *Geophys. J. Int.,* **203,** 943–959.

Cambiotti, G., Bordoni, A., Sabadini, R. & Colli, L., 2011a. Grace gravity data help constraining seismic models of the 2004 sumatran earthquake, *J. geophys. Res.,* **116,** B10403, doi:10.1029/2010JB007848.

Cambiotti, G., Ricard, Y. & Sabadini, R., 2011b. Ice age true polar wander in a compressible and non-hydrostatic earth, *Geophys. J. Int.,* **183,** 1284–1264.

Chambat, F., Ricard, Y. & Valette, B., 2010. Flattening of the earth: further from hydrostaticity than previously estimated, *Geophys. J. Int.,* **183,** 727–732.

Chao, B. & Gross, R., 1987. Changes in the earth's rotation and low-degree gravitational field induced by earthquakes, *Geophys. J. R. astr. Soc.,* **91,** 569–596.

Chao, B., Gross, R. & Han, Y., 1996. Seismic excitation of polar motion, 1977–1993, *Pure appl. Geophys.,* **146,** 407–419.

Dahlen, F., 1973. A correction to the excitation of the Chandler wobble by earthquakes, *Geophys. J. R. astr. Soc.,* **32,** 203–217.

Davies, G. & Brune, J., 1971. Regional and global fault slip rates from seismicity, *Nature,* **229,** 101–107.

Dziewonski, A. & Anderson, D., 1981. Preliminary reference earth model, *Phys. Earth planet. Inter.,* **25,** 297–356.

Dziewonski, A., Chou, T.-A. & Woodhouse, J., 1981. Determination of earthquake source parameters from waveform data for studies of global and regional seismicity, *J. geophys. Res.,* **86,** 2825–2852.

Ekström, G., Nettles, M. & Dziewonski, A., 2012. The global CMT project 2004–2010: centroid-moment tensors for 13,017 earthquakes, *Phys. Earth planet. Inter.,* **200–201,** 1–9.

Gross, R. & Chao, B., 2006. The rotational and gravitational signature of the December 26, 2004 Sumatran earthquake, *Surv. Geophys.,* **27,** 615–632.

Kagan, Y., 2002. Seismic moment distribution revisited: I. Statistical results, *Geophys. J. Int.,* **148,** 520–541.

Kagan, Y., 2014. *Earthquakes: Models, Statistics, Testable Forecasts,* American Geophysical Union.
Kagan, Y. & Jackson, D., 2013. Tohoku earthquake: a surprise?, *Bull. seism. Soc. Am.,* **103,** 1181–1194.
Kanamori, H., 1970. The Alaska Earthquake of 1964: radiation of long-period surface waves and source mechanism, *J. geophys. Res.,* **75,** 5029–5040.
Kanamori, H. & Cipar, J., 1974. Focal process of the great Chilean earthquake May 22, 1960, *Phys. Earth planet. Inter.,* **9,** 128–136.
Lambeck, K., 1980. *The Earth's Variable Rotation,* Cambridge Univ. Press.
Mansinha, L. & Smylie, D., 1967. Effect of earthquakes on the Chandler wobble and secular polar shift, *J. geophys. Res.,* **72,** 4731–4743.
McCaffrey, R., 2002. Crustal block rotations and plate coupling, in *Plate Boundary Zones,* pp. 101–122, eds Stein, S. & Freymueller, J., American Geophysical Union Geodynamics Series 30.
McCarthy, D. & Luzum, B., 1996. Path of the mean rotational pole from 1899 to 1994, *Geophys. J. Int.,* **125,** 623–629.
Meade, B. & Hager, B., 2005. Block models of crustal motion in southern California constrained by GPS measurements, *J. geophys. Res.,* **110,** B03403, doi:10.1029/2004JB003209.
Munk, W. & MacDonald, G., 1960. *The Rotation of the Earth,* Cambridge Univ. Press.
Murray, M. & Segall, P., 2001. Modeling broadscale deformation in northern california and nevada from plate motions and elastic strain accumulation, *Geophys. Res. Lett.,* **28,** 4315–4318.
Nakada, M., Okuno, J., Lambeck, K. & Purcell, A., 2015. Viscosity structure of earth's mantle inferred from rotational variations due to GIA process and recent melting events, *Geophys. J. Int.,* **202,** 976–992.
Obara, K., 2002. Nonvolcanic deep tremor associated with subduction in southwest Japan, *Science,* **296,** 1679–1681.
O'Connell, R. & Dziewonski, A., 1976. Excitation of the Chandler wobble by large earthquakes, *Nature,* **262,** 259–262.
Prawirodirdjo, L. *et al.*, 1997. Geodetic observations of interseismic strain segmentation at the Sumatra subduction zone, *Geophys. Res. Lett.,* **24,** 2601–2604.
Ranalli, G., 1995. *Rheology of the Earth,* 2nd edn, Chapman & Hall.
Savage, J., 1983. A dislocation model of strain accumulation and release at a subduction zone, *J. geophys. Res.,* **88,** 4984–4996.
Savage, J. & Burford, R., 1973. Geodetic determination of relative plate motion in central California, *J. geophys. Res.,* **78,** 832–845.
Segall, P., 2010. *Earthquake and Volcano Deformation,* Princeton Univ. Press.
Shelly, R., Peng, Z., Hill, D. & C., A., 2011. Triggered creep as a possible mechanism for delayed dynamic triggering of tremor and earthquakes, *Nat. Geosci.,* **4,** 384–388.
Smylie, D. & Zuberi, M., 2009. Free and forced polar motion and modern observations of the Chandler wobble, *J. Geodyn.,* **48,** 226–229.
Smylie, D., Mansinha, L. & Chapman, C., 1979. Seismic excitation of the chandler wobble revisited, *Geophys. J. R. astr. Soc.,* **59,** 1–17.
Smylie, D.E. & Mansinha, L., 1968. Earthquakes and the observed motion of the rotation pole, *J. geophys. Res.,* **73,** 7661–7673.
Smylie, D.E., Henderson, G.A. & Zuberi, M., 2015. Modern observations of the effect of earthquakes on the chandler wobble, *J. Geodyn.,* **83,** 85–91.
Soldati, G. & Spada, G., 1999. Large earthquakes and earth rotation: the role of mantle relaxation, *Geophys. Res. Lett.,* **26,** 911–914.
Soldati, G., Boschi, L., Piersanti, A. & Spada, G., 2001. The effect of global seismicity on the polar motion of a viscoelastic earth, *J. geophys. Res.,* **106,** 6761–6767.
Spada, G., 1997. Why are earthquakes nudging the pole towards 140°E, *Geophys. Res. Lett.,* **24,** 539–542.
Storchak, D.A., Di Giacomo, D., Bondar, I., Engdahl, E.R., Harris, J., Lee, W.H.K., Villaseqor, A. & Bormann, P., 2013. Public release of the ISC-GEM Global Instrumental Earthquake Catalogue (1900–2009), *Seismol. Res. Lett.,* **84,** 810–815.
Tsai, V., Nettles, M., Ekström, G. & Dziewonski, A., 2005. Multiple CMT source analysis of the 2004 Sumatra earthquake, *Geophys. Res. Lett.,* **32,** L17304, doi:10.1029/2005GL023813.
Xu, C., Sun, W. & Chao, B., 2014. Formulation of coseismic changes in earth rotation and low-degree gravity field based on the spherical earth dislocation theory, *J. geophys. Res.,* **119,** 9031–9041.
Yuen, D. & Peltier, W., 1982. Normal modes of the viscoelastic earth, *Geophys. J. Int.,* **69,** 495–526.
Zhou, J., Sun, W., Sun, H. & Xu, J., 2013. Reformulation of co-seismic polar motion excitation and low degree gravity changes: applied to the 2011 Tohoku-oki earthquake (M_w9.0), *J. Geogyn.,* **63,** 20–26.

SUPPORTING INFORMATION

Additional Supporting Information may be found in the online version of this paper:

Figure S1. The contribution to polar motion since 1976 due to (a) polar, (b) bipolar and (c) quadrupolar patterns of the seismic perturbation. The black line represents the contribution from the whole CMT catalogue and the grey line only that from interplate earthquakes (depth less than 70 km and within 220 km from plate boundaries). The amplitude of polar motion due to the (d) polar, (e) bipolar and (f) quadrupolar patterns is also shown.
Figure S2. As in Fig. S1, but black and grey lines represent the contributions from intraplate (depth less than 50 km and far from plate boundaries more than 220 km) and deep (depth greater than 50 km) earthquakes, respectively (http://gji.oxfordjournals.org/lookup/suppl/doi:10.1093/gji/ggw077/-/DC1)

Please note: Oxford University Press is not responsible for the content or functionality of any supporting materials supplied by the authors. Any queries (other than missing material) should be directed to the corresponding author for the paper.

APPENDIX A: PERTURBATION OF THE EARTH INERTIA DUE TO A POINT-LIKE SEISMIC SOURCE

From the MacCullagh formula (Munk & MacDonald 1960; Lambeck 1980; Chao & Gross 1987) or eqs (44) and (45) of Cambiotti & Sabadini (2015), the components ΔI_{13} and ΔI_{23} of the Earth inertia tensor $\Delta\mathbf{I}$ are related to the Stokes coefficients $\Delta X_{\ell m}$ of spherical harmonic degree $\ell = 2$ and order $m = \pm 1$ as follows:

$$\Delta I_{13} = -\sqrt{\frac{5}{3}}\, M_{\rm E}\, a^2\, \Delta X_{2-1} \tag{A1a}$$

$$\Delta I_{23} = -\sqrt{\frac{5}{3}}\, M_{\rm E}\, a^2\, \Delta X_{21}. \tag{A1b}$$

Here, for brevity, we agree with the convention that the negative, $m = -1$, and positive, $m = 1$, orders correspond to the Stokes coefficients of the cosine, $\Delta X_{2-1} = \Delta C_{21}$, and sine, $\Delta X_{21} = \Delta S_{21}$, type, respectively. Furthermore, by specifying eqs (30) and (43) of Cambiotti & Sabadini (2015) to the case of a point-like seismic source, these Stokes coefficients can be expressed in terms of the seismic Love number $k^{\rm D}_{2,p}$ as follows:

$$\Delta X_{2\pm1} = \sum_{p=0}^{2} k^{\rm D}_{2,p}(r)\, \frac{A^p_{2\pm1}}{a^3\, \mu(r)}, \tag{A2}$$

where $\mu(r)$ is shear modulus evaluated at the radius r of the seismic source, and $A^p_{2\pm1}$ ($p = 0, 1, 2$) are factors which depend on the colatitude, θ, and longitude, φ, of the epicentre, and on the seismic moment tensor $\mathbf{M}$. Their expression are listed hereinafter

$$A^p_{2\pm1} = \frac{M_p\, F^p_{2\pm1}(\theta,\varphi) + M_{-p}\, F^{-p}_{2\pm1}(\theta,\varphi)}{1+\delta_{p,0}}. \tag{A3}$$

Here, δ_{ij} is the Kronecker delta, $F^p_{2\pm1}$ ($p = -2, \ldots, 2$) are defined by eq. (18) and M_p ($p = -2, \ldots, 2$) are the following components (or combinations of components) of the seismic moment tensor, **M**, in the epicentral reference frame

$$M_0 = \frac{1}{3}\left(2\,M_{rr} - M_{\theta\theta} - M_{\varphi\varphi}\right) \tag{A4a}$$

$$M_{-1} = M_{\theta r} \tag{A4b}$$

$$M_1 = M_{\varphi r} \tag{A4c}$$

$$M_{-2} = \frac{1}{2}\left(M_{\theta\theta} - M_{\varphi\varphi}\right) \tag{A4d}$$

$$M_2 = M_{\theta\varphi}. \tag{A4e}$$

Substituting eqs (24) and (A4) into eq. (A1), we thus obtain eq. (5) with the non-dimensional factors B^p_1 ($p = 0, 1, 2$) given by

$$B^p_1 = -\sqrt{\frac{5}{3}}\,\frac{A^p_{2-1}}{a^3\,\mu(r)} \tag{A5a}$$

$$B^p_2 = -\sqrt{\frac{5}{3}}\,\frac{A^p_{21}}{a^3\,\mu(r)}. \tag{A5b}$$

Note that we only consider the perturbation of the Stokes coefficients due to the deviatoric part of the seismic moment tensor just because the CMT solution sets to zero the isotropic part. For the sake of completeness, we report hereinafter the perturbation of the Stokes coefficients due to the only isotropic part of the seismic moment tensor, although it does not enter in the simulations discussed in the main text

$$\Delta X_{2\pm1} = k^C_2(r)\,\frac{M_{rr} + M_{\theta\theta} + M_{\varphi\varphi}}{3\,\kappa(r)\,a^3}\,F^0_{2\pm1}(\theta, \varphi), \tag{A6}$$

where $\kappa(r)$ is the bulk modulus evaluated at the seismic source radius and k^C_2 is the gravitational seismic Love numbers governing the local incremental gravitational potential at the Earth surface associated with the isotropic part (Cambiotti & Sabadini 2015).

It is also useful to consider eq. (A4) in terms of the strike, ψ, dip, α and rake, γ, angles and seismic moment, M_s, for the case in which the seismic moment tensor can be interpreted as a double couple. In that case, we have

$$M_0 = M_s\,\sin(2\,\alpha)\,\sin(\gamma) \tag{A7a}$$

$$M_{-1} = -M_s\,(\cos(\alpha)\cos(\gamma)\cos(\psi) + \cos(2\alpha)\sin(\gamma)\sin(\psi)) \tag{A7b}$$

$$M_1 = M_s(\cos(\alpha)\cos(\gamma)\sin(\psi) - \cos(2\alpha)\sin(\gamma)\cos(\psi)) \tag{A7c}$$

$$M_{-2} = M_s\left(\frac{1}{2}\,\sin(2\alpha)\sin(\gamma)\cos(2\psi) - \sin(\alpha)\cos(\gamma)\sin(2\psi)\right) \tag{A7d}$$

$$M_2 = -M_s\left(\sin(\alpha)\cos(\gamma)\cos(2\psi) + \frac{1}{2}\,\sin(2\alpha)\sin(\gamma)\sin(2\psi)\right) \tag{A7e}$$